ACS Sustainable Chemistry & Engineering

Research Article

pubs.acs.org/journal/ascecg

Light-Induced Open Circuit Voltage Increase in Polymer Solar Cells with Ternary Bulk Heterojunction Nanolayers

Sungho Nam,[†] Sooyong Lee,[†] Jaehoon Jeong,[†] Jooyeok Seo,[†] Hwajeong Kim,*[,†,‡] Dong-Ik Song,[§] and Youngkyoo Kim*[,†]

[†]Organic Nanoelectronics Laboratory, School of Applied Chemical Engineering, Kyungpook National University, University Road 80, Buk-gu, Daegu 702-701, Republic of Korea

[‡]Research Institute of Advanced Energy Technology, Kyungpook National University, University Road 80, Buk-gu, Daegu 702-701, Republic of Korea

[§]Polymer Rheology Laboratory, School of Applied Chemical Engineering, Kyungpook National University, University Road 80, Buk-gu, Daegu 702-701, Republic of Korea

S *Supporting Information*

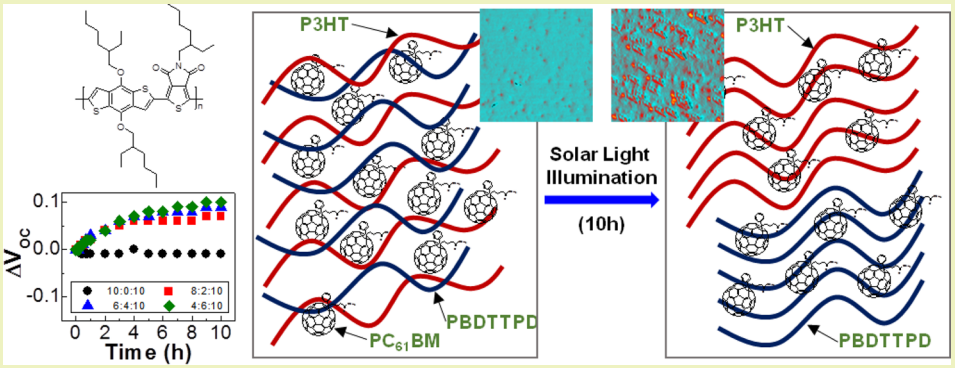

ABSTRACT: We report a light-induced open circuit voltage (V_{OC}) increase in polymer solar cells with ternary bulk heterojunction (BHJ) layers that are composed of poly(3-hexylthiophene) (P3HT), poly[(4,8-bis(2-ethylhexyloxy)-benzo[1,2-b:4,5-b′]dithiophene)-2,6-diyl-*alt*-(N-2-ethylhexylthieno[3,4-*c*]pyrrole-4,6-dione)-2,6-diyl]] (PBDTTPD), and [6,6]-phenyl-C_{61}-butyric acid methyl ester ($PC_{61}BM$). The ternary BHJ layers were prepared by varying the composition of donor polymers at a fixed ratio (1:1 by weight) of donor (P3HT + PBDTTPD) to acceptor ($PC_{61}BM$). Results showed that V_{OC} was gradually increased under continuous illumination of solar light (100 mW/cm^2) for ternary solar cells, whereas no V_{OC} increase was measured for binary solar cells without PBDTTPD. As a consequence, the power conversion efficiency (PCE) of ternary solar cells (except the highest PBDTTPD content) was rather higher after solar light illumination for 10 h, even though the binary solar cell exhibited significantly lowered PCE after 10 h illumination. The V_{OC} increase has been attributed to the lateral phase segregation between P3HT and PBDTTPD domains in the ternary BHJ layers under continuous illumination of solar light, as evidenced from the analysis result by Raman spectroscopy, atomic force microscopy, transmission electron microscopy, and synchrotron radiation grazing-incidence angle X-ray diffraction measurements.

KEYWORDS: *Polymer solar cells, Ternary BHJ, Light-induced, Open circuit voltage, PBDTTPD*

INTRODUCTION

Polymer solar cells with bulk heterojunction (BHJ) layers of electron-donating conjugated polymers and electron-accepting fullerene derivatives, which are basically solution processable, have been extensively studied because of their potential for cost-effective manufacturing of lightweight and flexible solar modules by employing continuous roll-to-roll processes.[1−10] The power conversion efficiency (PCE) of polymer:fullerene solar cells has reached 8−10% due to new conjugated polymers with low band gaps and/or deep highest occupied molecular orbital (HOMO) energy levels.[11−13]

Although such new conjugated polymers have been recently introduced, regioregular poly(3-hexylthiophene) (P3HT) is still considered one of the most attractive electron-donating polymers because it can deliver 4−5% PCE by making a BHJ layer with soluble fullerene derivatives such as [6,6]-phenyl-C_{61}-butyric acid methyl ester ($PC_{61}BM$).[14−17] In particular, the P3HT polymer exhibited ∼7% PCE in combination with an indene-C_{60} bisadduct (ICBA) featuring a lower energy level of a

Received: August 5, 2014
Revised: November 21, 2014
Published: December 17, 2014

lowest unoccupied molecular orbital (LUMO) leading to an open circuit voltage (V_{OC}) increase.[18,19]

However, despite the improved performance of polymer:-fullerene solar cells, their stability issue has been still unresolved so that it has been a hurdle for commercialization. The poor device stability can be ascribed to three major reasons: (1) corrosion of transparent electrodes caused by strong acidity of hole collecting buffer layer (HCBL), (2) degradation of conjugated polymers under solar light, and (3) morphological instability in the BHJ layers and/or recrystallization of fullerene derivatives.[20−24] For such reasons, the morphological instability, which may be closely related to the gradual demixing (phase segregation) between conjugated polymers and fullerene derivatives, is regarded as the most critical bottleneck for achieving the stability of polymer:fullerene solar cells.[24−27] The morphology change by the thermally induced $PC_{61}BM$ crystallization within the P3HT:$PC_{61}BM$ blend films has been reported,[25,26] while the light-induced morphology change leading to the $PC_{61}BM$ aggregation has been reported for the P3HT:$PC_{61}BM$ blend film even though the glass transition temperatures of P3HT were considerably higher than typical temperatures of solar cells under solar light.[27]

In this work, as an alternative approach for the stability improvement in the polymer:fullerene solar cells, we attempted to introduce a third polymer to the P3HT:$PC_{61}BM$ blends in order to investigate the role of the third component (polymer) on the stability of solar cells. As the third component, poly[(4,8-bis(2-ethylhexyloxy)-benzo[1,2-b:4,5-b′]-dithiophene)-2,6-diyl-*alt*-(N-2-ethylhexylthieno[3,4-*c*]pyrrole-4,6-dione)-2,6-diyl]] (PBDTTPD) was used in consideration of its energy band structure because its addition resulted in a significant PCE enhancement in the case of the P3HT:$PC_{61}BM$ solar cells with a low fullerene content (P3HT:$PC_{61}BM$ = 1:0.5 by weight) in our recent report.[28] In the present study, unlike the previous work, the weight ratio of polymers (P3HT + PBDTTPD) to $PC_{61}BM$ was fixed as 1:1 by weight because this composition has been confirmed to deliver one of the best PCEs for the P3HT:$PC_{61}BM$ solar cells. The resulting ternary solar cells were examined by measuring the device performances under continuous (10 h) illumination of solar light (100 mW/cm^2). As a result, all ternary solar cells exhibited noticeably increased V_{OC} leading to the improved PCE even after the 10 h illumination.

EXPERIMENTAL SECTION

Materials and Solutions. The regioregular P3HT polymer was purchased from Rieke Metal, Inc. The regioregularity, weight-average molecular weight ($\overline{M_W}$), and polydispersity index (PDI) of the P3HT polymer were 91%, 6.2 × 10^4 Da, and 2.3, respectively. The PBDTTPD polymer ($\overline{M_W}$ = 1.3 × 10^5 Da, PDI = 2.5) was supplied from Solarmer Materials, Inc. $PC_{61}BM$ was received from Nano-C and used without further purification, while the PEDOT:PSS solution (PH500) was purchased from H. C. Starck. The chemical structures of materials are shown in Figure 1a. Binary and ternary blend solutions were prepared using chlorobenzene as a solvent at a solid concentration of 20 mg/mL by varying the ratio of the two polymers at a fixed ratio of polymers (P3HT + PBDTTPD) to $PC_{61}BM$ (P3HT:PBDTTPD:$PC_{61}BM$ = 10−*X*:*X*:10 by weight, where *X* = 0, 2, 4, 6). These binary and ternary blend solutions were vigorously stirred on a magnetic stirring plate for 24 h before spin-coating.

Thin film and Device Fabrication. Indium−tin oxide (ITO)-coated glass substrates were patterned to make the ITO electrodes by employing photolithography/etching process. The patterned ITO−glass substrates were cleaned using acetone and isopropyl alcohol using an ultrasonic cleaner and dried with a nitrogen flow. The dried

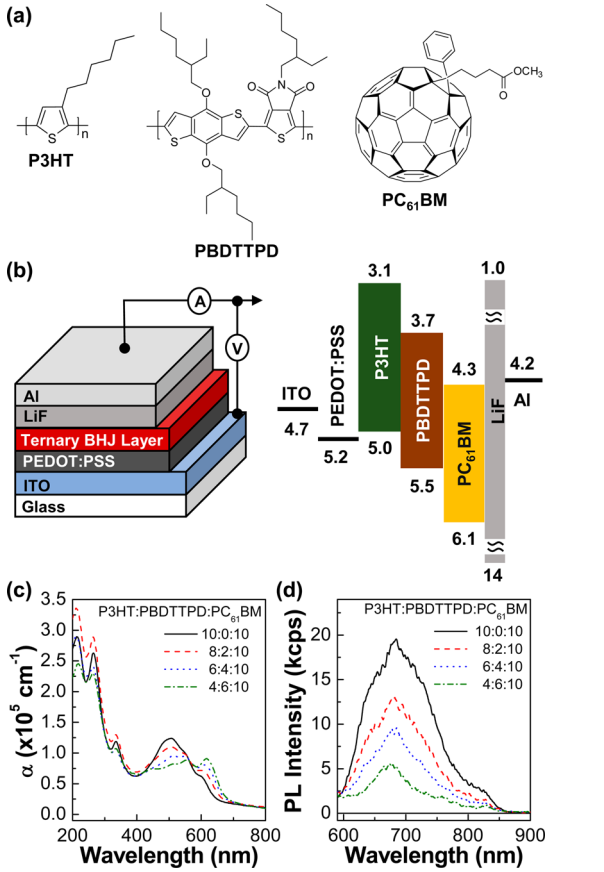

Figure 1. (a) Chemical structure of materials used in this work. (b) Illustration of device structure (left) and flat energy band diagram for the device with the ternary BHJ layer (right). Note that the energy unit (eV) and minus sign (−) were omitted. (d) Optical absorption coefficient (α) and (e) photoluminescence spectra (excitation at 505 nm) for binary and ternary bulk heterojunction films coated on quartz substrates.

ITO−glass substrates were treated inside a UV−ozone cleaner for 20 min in order to remove any remnant organic residues on the surface of the substrates as well as to make the ITO surface hydrophilic. Then the PEDOT:PSS layer (thickness = 60 nm) was spin-coated on top of the ITO−glass substrates, followed by thermal annealing at 200 °C for 15 min. To make active layers, the binary and ternary blend layers (thickness = 60 nm) were spin-coated on the PEDOT:PSS layers and soft-baked at 60 °C for 15 min. These film-coated samples were transferred to a vacuum chamber in an argon-filled glovebox. After pumping the chamber pressure down to ∼1 × 10^{-6} Torr, lithium fluoride (LiF, thickness = ∼1 nm) and aluminum (Al, thickness = 80 nm) were sequentially deposited on top of the active layers through a shadow mask. The active area of the devices fabricated in this work was 0.09 cm^2. The device structure is shown in Figure 1b (left). Finally, all devices were subject to thermal annealing at 150 °C for 10 min and stored inside the same glovebox before measurements. For the morphology and nanostructure measurements, all samples were prepared in the same way as for the device fabrication, whereas the film samples were prepared by spin-coating on quartz substrates for optical measurements.

Measurements. The thicknesses of the thin films were measured using a surface profiler (Alpha Step 200, Tencor Instruments). The optical absorption and photoluminescence spectra of the active layers were measured using a UV−visible spectrometer (Optizen 2120, MECASYS) and a photoluminescence (PL) spectrometer (FS-2, SCINCO), respectively. The Raman spectra of the thin films were measured using a Raman spectrometer (Almega X, Thermo). The surface morphologies of the film samples were measured using an

dx.doi.org/10.1021/sc500505t | ACS Sustainable Chem. Eng. 2015, 3, 55−62

atomic force microscope (AFM, Nanoscope IIIa, Digital Instruments), while the nanostructures of the film samples were measured using a synchrotron radiation-grazing incidence X-ray diffraction (GIXD) system (X-ray wavelength = 0.11352 nm, incidence angle = 0.12°, 3C SAXS I beamline, Pohang Accelerator Laboratory) and a high-resolution transmission electron microscope (HRTEM, HT 7700, Hitachi). The performance of the solar cells under 1 sun condition (100 mW/cm^2) was measured using a specialized solar cell measurement system equipped with a solar simulator (92250A-1000, Newport-Oriel) and an electrometer (Model 2400, Keithley). The current density−voltage (*J-V*) curves of the devices in the dark were measured using the same electrometer in the solar cell measurement system. The short time stabilities of the devices in an argon environment were measured under illumination of solar light (100 mW/cm^2) for 10 h.

RESULTS AND DISCUSSION

Considering the quite large offset (~0.6 eV) of the lowest unoccupied molecular orbital (LUMO) energy for the three components (see the ideal flat energy band diagram in Figure 1b, right),[29,30] the third component (PBDTTPD) is expected to play an intermediate role in the charge separation/transfer process between P3HT and $PC_{61}BM$ components for the present devices with a high fullerene content (P3HT:$PC_{61}BM$ = 1:1 by weight) (note that the LUMO energy value of −4.3 eV was used for $PC_{61}BM$ because most of $PC_{61}BM$ molecules are considered to be aggregated to each other in the binary and ternary films[31−34]). This assumption is evident from the result that the PL intensity was gradually reduced as the PBDTTPD content increased (Figure 1d). Here, we note that the overall PL intensity should be maintained or increased by the PL of PBDTTPD, which is brighter than P3HT (Figure S1, Supporting Information), if no charge separation process was made and/or any Förster energy transfer from P3HT to PBDTTPD components has occurred (even though the Förster energy transfer seems to be very small when it comes to the band gap energy of the two polymers (E_g = 1.9 eV for P3HT, 1.8 eV for PBDTTPD) from the optical absorption spectra in Figure S2 of the Supporting Information).[35−38] Although the PBDTTPD component was expected to ideally play an intermediate role in the charge separation/transfer process, the performance of the ternary blend (P3HT:PBDTTPD:$PC_{61}BM$) solar cell was relatively inferior to that of the binary (P3HT:$PC_{61}BM$) solar cell (Figure S3 and Table S1, Supporting Information), which can be attributed to the relatively poor charge transport for the ternary solar cells as evidenced from their high series resistances under illumination of solar light (Table S1, Supporting Information) and the dark *J-V* curves (Figure S4, Supporting Information).

As shown in Figure 2, a noticeable increase in the open circuit voltage (V_{OC}) was measured for all ternary solar cells under continuous illumination of solar light (100 mW/cm^2), even though the V_{OC} value was rather decreased with time for the binary solar cell. We note that only a single work on the V_{OC} increase by post-treatment after device fabrication has been reported for the physical pressing of solar cells with the LiF layer.[39] However, the trend of short circuit current density (J_{SC}) was similar for both binary and ternary solar cells. To find any clue of the J_{SC} reduction under continuous illumination of solar light, the color of the active (BHJ) layers was examined, but it was almost not changed for all film samples as shown in the inset photographs in Figure 2. This result may imply that the photoinduced degradation of polymers (P3HT and PBDTTPD) under continuous illumination of solar light is

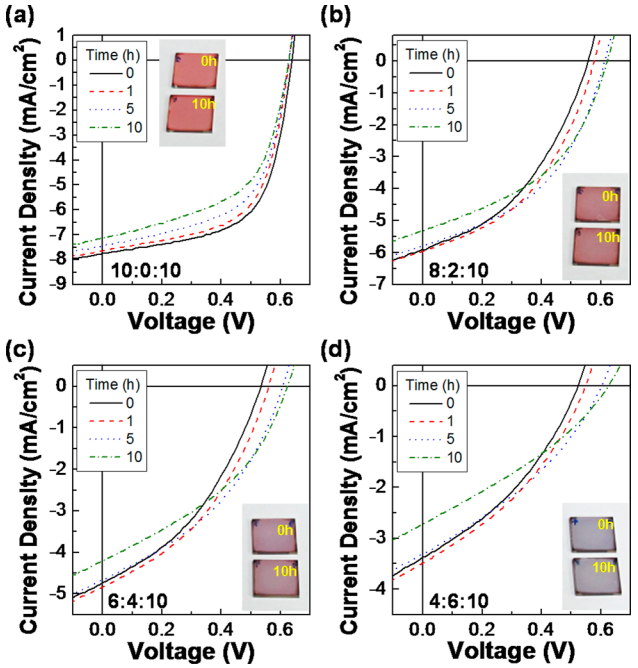

Figure 2. Light *J-V* curves for binary and ternary solar cells according to the illumination time under 1 sun conditions (100 mW/cm^2): (a) P3HT:PBDTTPD:$PC_{61}BM$ = 10:0:10, (b) P3HT:PBDTTPD:$PC_{61}BM$ = 8:2:10, (c) P3HT:PBDTTPD:$PC_{61}BM$ = 6:4:10, and (d) P3HT:PBDTTPD:$PC_{61}BM$ = 4:6:10. Insets in each graph show the photographs for the binary and ternary BHJ films before and after 10 h illumination.

not a major reason for the J_{SC} reduction, which is supported by the optical properties before and after 10 h illumination (Figures S5 and S6, Supporting Information).

To further investigate the performance change of ternary solar cells under continuous illumination of solar light, the detailed trend of solar cell parameters as a function of illumination time was plotted in Figure 3. The V_{OC} value was gradually increased with the illumination time for all ternary solar cells, whereas it was slightly negative for the binary solar cell. In particular, the V_{OC} increase in the ternary (4:6:10) solar cell was ~0.1 V (from 0.52 to 0.62 V) by 10 h illumination (Table S2, Supporting Information), which corresponds to about a 19% increase in V_{OC}. Here, it is noteworthy that the final V_{OC} value reached 0.62 V for all ternary solar cells, which may indicate the possible limit of V_{OC} in the present device structure upon illumination of solar light. In addition to the V_{OC} increase, the J_{SC} value was also initially (up to 1 h) increased for all ternary solar cells, whereas the binary solar cell exhibited a gradual reduction in J_{SC}. Moreover, the fill factor (FF) was slightly increased with time for the ternary (8:2:10) solar cell and was well maintained for the ternary (6:4:10) solar cell, whereas it was gradually decreased with time for the binary solar cell. As a consequence, the PCE of ternary solar cells (8:2:10 and 6:4:10) was rather higher after 10 h illumination of solar light than that of the fresh devices (note that the maximum PCE was obtained at around 3−5 h for these two ternary solar cells), whereas the PCE of the binary solar cell was gradually decreased with illumination time.

To understand the impressive performance increase for the ternary solar cells, the surface morphology of blend films was briefly examined with atomic force microscopy. As shown in Figure 4, the surface morphology of the binary blend film was

dx.doi.org/10.1021/sc500505t | ACS Sustainable Chem. Eng. 2015, 3, 55−62

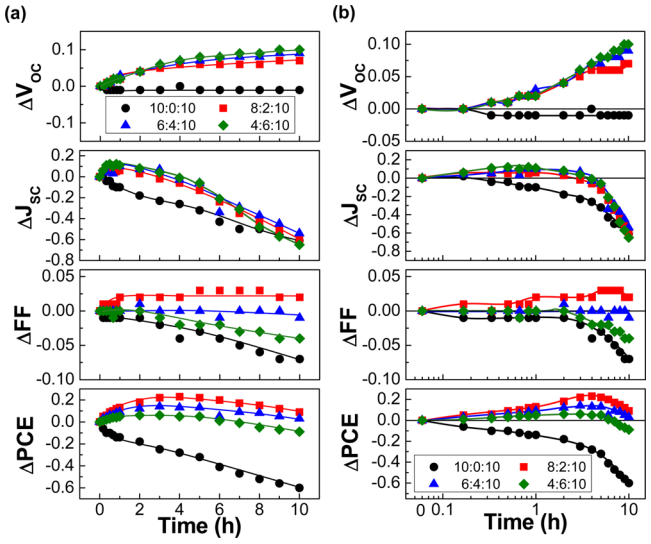

Figure 3. Change of V_{OC}, J_{SC}, FF, and PCE as a function of illumination time for binary and ternary solar cells: (a) linear scale and (b) semilogarithmic scale. The composition for the BHJ layers is given in the top in panel (a) and in the bottom in panel (b): (black circles) P3HT:PBDTTPD:$PC_{61}BM$ = 10:0:10, (red squares) P3HT:PBDTTPD:$PC_{61}BM$ = 8:2:10, (blue triangles) P3HT:PBDTTPD:$PC_{61}BM$ = 6:4:10, and (green diamonds) P3HT:PBDTTPD:$PC_{61}BM$ = 4:6:10.

marginally changed, but a more pronounced morphology change was measured for the ternary blend film (8:2:10) after 10 h illumination. This is evident from the different root-mean-square roughness (R_g) changes, such as 0.85 to 0.98 nm (15% increase) for the binary blend film and 2.69 to 3.62 nm for the ternary blend film (35% increase). Here, we note that the surface of the ternary blend film was already much coarser than that of the binary blend film before solar light illumination. This reflects that the addition of 10 wt % PBDTTPD did greatly affect the surface morphology of blend films and is considered to be responsible for the gradual V_{OC} increase upon solar light illumination.

However, the surface morphology change itself cannot account for the V_{OC} increase in the present ternary solar cells, so we employed a Raman back scattering technique because of its capability for qualitative measurement on the chemical composition in the surface region of thin films.[40] As shown in Figure 5, the characteristic Raman peaks for P3HT (1375 cm^{-1} for the C−C skeletal stretch mode and 1442 cm^{-1} for the C═C symmetric stretch mode in Figure S7 of the Supporting Information)[26,40−43] were almost marginally changed after 10 h illumination for the binary blend film, which is in good agreement with the AFM result in Figure 4. In contrast, the ternary (8:2:10) blend film showed noticeable changes in the Raman intensity after 10 h illumination. The representative P3HT peaks at 1375 and 1442 cm^{-1} were obviously decreased after 10 h illumination, whereas the PBDTTPD peaks at 1477 and 1517 cm^{-1} were pronouncedly increased. This result does directly indicate that the PBDTTPD composition became relatively enriched in the surface region of the ternary blend film, which further implies that the enriched PBDTTPD component might be the pop-up nanodomains grown after 10 h illumination in the AFM image (Figure 4b, right). This assumption is supported from the TEM image (Figure 6) because the darker domains in Figure 6b are obviously different from the nanoscale morphology of the binary (P3HT:$PC_{61}BM$) blend film in Figure 6a. Here,

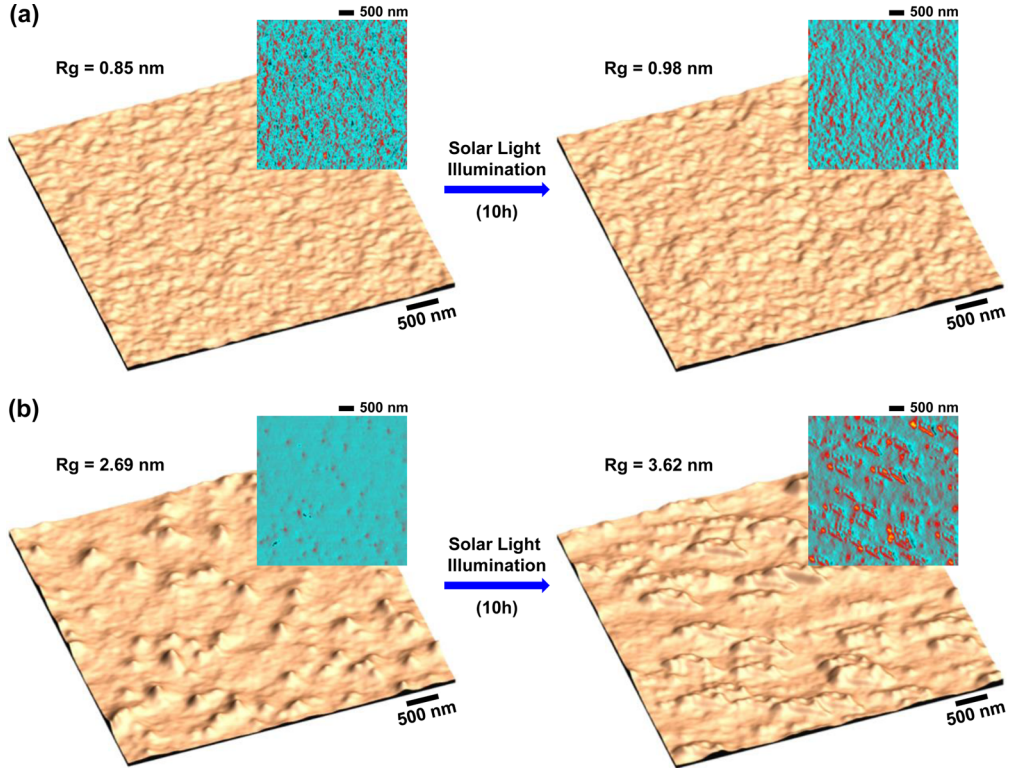

Figure 4. 3D height-mode AFM images (2D phase mode: upper right) for (a) binary (P3HT:PBDTTPD:$PC_{61}BM$ = 10:0:10) and (b) ternary (P3HT:PBDTTPD:$PC_{61}BM$ = 8:2:10) BHJ layers before and after 10 h solar light illumination.

dx.doi.org/10.1021/sc500505t | ACS Sustainable Chem. Eng. 2015, 3, 55−62

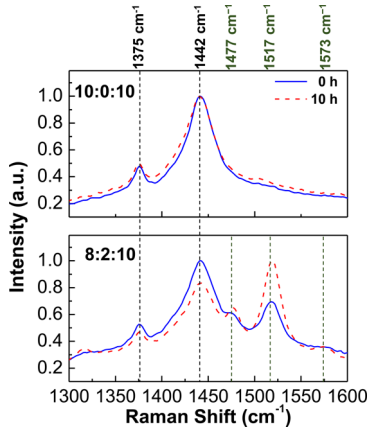

Figure 5. Raman spectra for (top) binary (P3HT:PBDTTPD:$PC_{61}BM$ = 10:0:10) and (bottom) ternary (P3HT:PBDTTPD:$PC_{61}BM$ = 8:2:10) BHJ layers before and after 10 h solar light illumination. The excitation wavelength was 780 nm for all samples.

particular attention is paid to the tiny black spots (<5 nm) in Figure 6a (right), which are considered as the $PC_{61}BM$ aggregates generated after 10 h illumination and are supposed to be one of the major reasons for the poor stability in the binary solar cell. In contrast, such $PC_{61}BM$ aggregates were not found in the present ternary blend film, which may support that the PBDTTPD component played a critical role in retarding the aggregation of $PC_{61}BM$ molecules in the blend film leading to better stability in the ternary solar cells.

This scenario can be also supported from the GIXD results in Figure 7. As observed from the 2D GIXD images for the binary blend film (Figure 7a), the characteristic Debye rings for the (100) and (200) diffraction of P3HT became more intense after 10 h illumination. This is clearly shown in the 1D GIXD profile for the binary blend because both the out-of-plane (OOP) and in-plane (IP) peak intensities of P3HT were

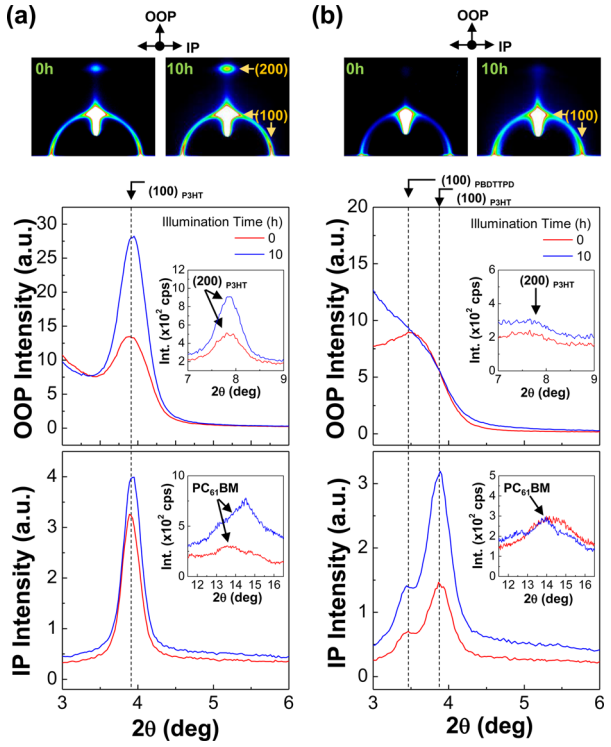

Figure 7. 2D GIXD images (top) and 1D GIXD profiles (bottom) for (a) binary (P3HT:PBDTTPD:$PC_{61}BM$ = 10:0:10) and (b) ternary (P3HT:PBDTTPD:$PC_{61}BM$ = 8:2:10) BHJ layers before and after 10 h solar light illumination. Note that the insets show the 1D GIXD profiles at higher diffraction angles in order to examine the (200) peak of P3HT (see the OOP intensity plot) and the $PC_{61}BM$ peak (see the IP intensity plot).

significantly increased after 10 h illumination. These results indicate that a further recrystallization process occurred for the P3HT chains in the binary blend film upon illumination of solar

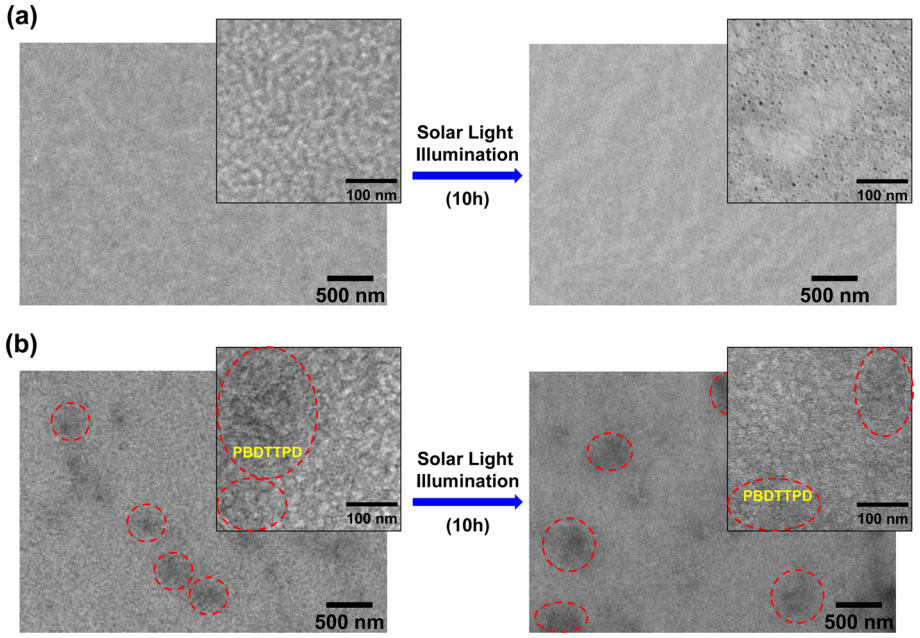

Figure 6. TEM images for (a) binary (P3HT:PBDTTPD:$PC_{61}BM$ = 10:0:10) and (b) ternary (P3HT:PBDTTPD:$PC_{61}BM$ = 8:2:10) BHJ layers before and after 10 h solar light illumination. Note that the insets (right top) are for the high-resolution images that were measured again by magnifying the TEM system.

dx.doi.org/10.1021/sc500505t | ACS Sustainable Chem. Eng. 2015, 3, 55−62

light for 10 h. In particular, the diffraction peak for $PC_{61}BM$ in the IP direction was measured for the binary blend film after 10 h illumination (inset, Figure 7a, bottom), which can be attributed to the $PC_{61}BM$ aggregates generated as discussed above. In the case of the ternary (8:2:10) blend film (Figure 7b), the major OOP diffraction peak position was corresponded to the PBDTTPD diffraction (2θ = 3.46°), but no individual P3HT peak was measured before light illumination, whereas the individual diffraction peaks for P3HT and PBDTTPD were certainly measured in the IP direction (Figure S8, Supporting Information). This result implies that both P3HT and PBDTTPD chains were relatively well mixed in the OOP direction by the addition of PBDTTPD in the ternary blend film, but a discrete phase segregation was made in the IP direction. This assumption is in good agreement with the nanomorphology featuring nanospots (domains) measured in the AFM and TEM images, although some parts of the PBDTTPD components might be still well mixed with the P3HT chains apart from these nanodomains. The IP diffraction peaks in the ternary blend film were increased after 10 h illumination, whereas the peak in the OOP direction did clearly lose its maximum peak position in the present measurement angle region. This result reflects that the phase segregation in the ternary blend film became pronounced for both IP and OOP directions after 10 h illumination leading to more individual polymer chain stacking, which agrees with the increased domain size in the AFM image (Figure 4b, right).

On the basis of above characterization results, we can draw a short conclusion that a laterally phase-segregated morphology was evolved in the present ternary blend films after 10 h illumination. In other words, before illumination, the coexistence (well-mixed state) of P3HT and PBDTTPD resulted in a relatively low V_{OC} because of the band offset (0.7 eV) between major components (P3HT and $PC_{61}BM$) as well as a possible charge-blocking resistance by the presence of the PBDTTPD chains in the P3HT domains. Under illumination of solar light, however, the lateral phase segregation process induced an additional individual BHJ combination (band offset = 1.1 eV) between PBDTTPD and $PC_{61}BM$ in the ternary blend films, which might contribute to a V_{OC} increase and device stability (Figure 8). Considering simply the V_{OC} value (up to 0.62 V) for all ternary devices after 10 h illumination (Table S2, Supporting Information), the P3HT:$PC_{61}BM$ components are expected to solely influence the V_{OC} increase. However, the stability trend suggests that both the P3HT:$PC_{61}BM$ component and the PBDTTPD:$PC_{61}BM$ component played a harmonic role in improving both device stability and V_{OC}.

CONCLUSIONS

Ternary polymer:fullerene solar cells were fabricated with ternary bulk heterojunction films of P3HT, PBDTTPD, and $PC_{61}BM$ by varying the composition of polymer components (PBDTTPD to P3HT) in order to investigate the influence of the third component (PBDTTPD) on the stability of polymer:fullerene solar cells. The ternary solar cells showed a gradual V_{OC} increase (in the presence of an initial J_{SC} increase) upon illumination of solar light, even though the initial performance of ternary solar cells was relatively poorer than that of the binary solar cell. As a result, the PCE of the binary solar cell was reduced by ~0.6% after 10 h illumination, whereas that of the ternary solar cell (8:2:10) was rather increased even after 10 h illumination. The reason for the V_{OC} increase in the ternary solar cells was assigned to the formation of lateral phase segregation morphology that contains two different individual BHJ units in the same device due to the evolution of an additional BHJ unit (between PBDTTPD and $PC_{61}BM$) to the existing BHJ unit between major components (P3HT and $PC_{61}BM$). In particular, the present ternary blend approach could prevent the formation of $PC_{61}BM$ aggregates, which was one of the critical problems for the poor stability in the binary polymer:fullerene solar cells. Further improvement can be achieved by changing the thermal annealing conditions, introducing inverted structures (to remove the PEDOT:PSS effect), and applying new conjugated polymers as a third component. Hence, we expect that the present idea could be a milestone work for improving the stability of polymer:fullerene solar cells in terms of morphological instability issues in the BHJ layers.

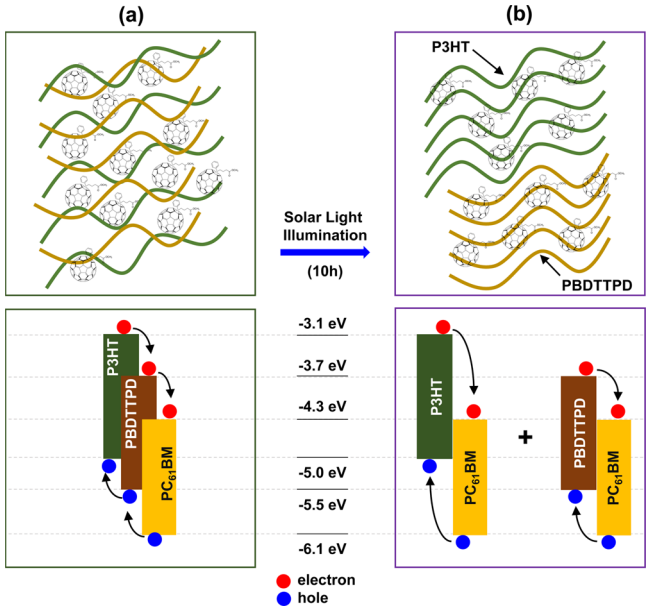

Figure 8. Proposed (ideal) morphology for the ternary BHJ layers (a) before and (b) after solar light illumination in order to explain the V_{OC} increase (note that the two BHJ components in panel (b) might be not perfectly isolated but closely correlated in real devices). The resulting flat energy band diagram (BHJ components only) is given on the bottom. The arrows denote the ideal transfer direction of electrons and holes at a short circuit condition (note that the energy band will be bended and deformed at a short circuit condition).

ASSOCIATED CONTENT

Supporting Information

Absorption coefficient and PL spectra of pristine films, solar cell performance according to PBDTTPD content and illumination time, light and dark *J-V* curves of all devices, optical density and PL spectra of BHJ films, Raman spectra, and 2D GIXD images and 1D GIXD profiles of pristine films. This material is available free of charge via the Internet at http://pubs.acs.org.

AUTHOR INFORMATION

Corresponding Authors

*E-mail: ykimm@knu.ac.kr. Tel: +82-53-950-5616.
*E-mail: khj217@knu.ac.kr.

Notes

The authors declare no competing financial interest.

■ ACKNOWLEDGMENTS

This work was financially supported by Korean Government grants: Basic Research Laboratory Program (2011-0020264), Pioneer Research Center Program (2012-0001262), Basic Science Research Program (2009-0093819), MOTIE (10048434), NRF (2012K1A3A1A09027883), and NRF (2012R1A1B3000523).

■ REFERENCES

(1) Dang, M. T.; Hirsch, L.; Wantz, G.; Wuest, J. D. Controlling the morphology and performance of bulk heterojunctions in solar cells. Lessons learned from the benchmark poly(3-hexylthiophene):[6,6]-phenyl-C61-butyric acid methyl ester system. *Chem. Rev.* **2013**, *113*, 3734−3765.

(2) Helgesen, M.; Søndergaard, R.; Krebs, F. C. Advanced materials and processes for polymer solar cell devices. *J. Mater. Chem.* **2010**, *20*, 36−60.

(3) Brabec, C. J.; Gowrisanker, S.; Halls, J. J. M.; Laird, D.; Jia, S.; Williams, S. P. Polymer−fullerene bulk-heterojunction solar cells. *Adv. Mater.* **2010**, *22*, 3839−3856.

(4) Beaujuge, P. M.; Fréchet, J. M. J. Molecular design and ordering effects in π-functional materials for transistor and solar cell applications. *J. Am. Chem. Soc.* **2011**, *133*, 20009−20029.

(5) Boudreault, P. L.; Najari, A.; Leclerc, M. Processable low-bandgap polymers for photovoltaic applications. *Chem. Mater.* **2011**, *23*, 456−469.

(6) Cabanetos, C.; Labban, A. E.; Bartelt, J. A.; Douglas, J. D.; Mateker, W. R.; Fréchet, J. M. J.; McGehee, M. D.; Beaujuge, P. M. Linear side chains in benzo[[1,2-b:4,5-b′]dithiophene−thieno[3,4-c]pyrrole-4,6-dione polymers direct self-assembly and solar cell performance. *J. Am. Chem. Soc.* **2013**, *135*, 4656−4659.

(7) Sun, Y.; Seifter, J.; Wang, M.; Perez, L. A.; Luo, C.; Bazan, G. C.; Huang, F.; Cao, Y.; Heeger, A. J. Effect of molecular order on the performance of naphthobisthiadiazole-based polymer solar cells. *Adv. Energy Mater.* **2014**, *4*, 1301601 DOI: 10.1002/aenm.201301601.

(8) Gélinas, S.; Rao, A.; Kumar, A.; Smith, S. L.; Chin, A. W.; Clark, J.; van der Poll, T. S.; Bazan, G. C.; Friend, R. H. Ultrafast long-range charge separation in organic semiconductor photovoltaic diodes. *Science* **2013**, *343*, 512−516.

(9) Bronstein, H.; Collado-Fregoso, E.; Hadipour, A.; Soon, Y. W.; Huang, Z.; Dimitrov, S. D.; Ashraf, R. S.; Rand, B. P.; Watkins, S. E.; Tuladhar, P. S.; Meager, I.; Durrant, J. R.; McCulloch, I. Thieno[3,2-*b*]thiophene-diketopyrrolopyrrole containing polymers for inverted solar cells devices with high short circuit currents. *Adv. Funct. Mater.* **2013**, *23*, 5647−5654.

(10) Liu, B.; Png, R. Q.; Zhao, L. H.; Chua, L. L.; Friend, R. H.; Ho, P. K. H. High internal quantum efficiency in fullerene solar cells based on crosslinked polymer donor networks. *Nat. Commun.* **2012**, *3*, 1321.

(11) Woo, S.; Kim, W. H.; Kim, H.; Yi, Y.; Lyu, H. K.; Kim, Y. 8.9% single-stack inverted polymer solar cells with electron-rich polymer nanolayer-modified inorganic electron-collecting buffer layers. *Adv. Energy Mater.* **2014**, *4*, 1301692.

(12) Guo, X.; Zhou, N.; Lou, S. J.; Smith, J.; Tice, D. B.; Hennek, J. W.; Ortiz, R. P.; Navarrete, J. T. L.; Li, S.; Strzalka, J.; Chen, L. X.; Chang, R. P. H.; Facchetti, A.; Marks, T. J. Polymer solar cells with enhanced fill factors. *Nat. Photonics* **2013**, *7*, 825−833.

(13) Zhang, M.; Gu, Y.; Guo, X.; Liu, F.; Zhang, S.; Huo, L.; Russell, T.; Hou, J. Efficient polymer solar cells based on benzothiadiazole and alkylphenyl substituted benzodithiophene with a power conversion efficiency over 8%. *Adv. Mater.* **2013**, *25*, 4944−4949.

(14) Kim, Y.; Choulis, S. A.; Nelson, J.; Bradley, D. D. C.; Cook, S.; Durrant, J. R. Device annealing effect in organic solar cells with blends of regioregular poly(3-hexylthiophene) and soluble fullerene. *Appl. Phys. Lett.* **2005**, *86*, 063502.

(15) Kim, Y.; Cook, S.; Tuladhar, S. M.; Choulis, S. A.; Nelson, J.; Durrant, J. R.; Bradley, D. D. C.; Giles, M.; Mcculloch, I.; Ha, C. S.; Ree, M. A strong regioregularity effect in self-organizing conjugated polymer films and high-efficiency polythiophene:fullerene solar cells. *Nat. Mater.* **2006**, *5*, 197−203.

(16) Ma, W.; Yang, C.; Gong, X.; Lee, K.; Heeger, A. J. Thermally stable, efficient polymer solar cells with nanoscale control of the interpenetrating network morphology. *Adv. Funct. Mater.* **2005**, *15*, 1617−1622.

(17) Li, G.; Shrotriya, V.; Huang, J. S.; Yao, Y.; Moriarty, T.; Emery, K.; Yang, Y. High-efficiency solution processable polymer photovoltaic cells by self-organization of polymer blends. *Nat. Mater.* **2005**, *4*, 864−868.

(18) He, Y.; Chen, H. Y.; Hou, J.; Li, Y. Indene-C60 bisadduct: A new acceptor for high-performance polymer solar cells. *J. Am. Chem. Soc.* **2010**, *132*, 1377−1382.

(19) Cheng, Y. J.; Hsieh, C. H.; He, Y.; Hsu, C. S.; Li, Y. Combination of Indene-C_{60} bis-adduct and cross-linked fullerene interlayer leading to highly efficient inverted polymer solar cells. *J. Am. Chem. Soc.* **2010**, *132*, 17381−17383.

(20) Kim, H.; Nam, S.; Lee, H.; Woo, S.; Ha, C. S.; Ree, M.; Kim, Y. Influence of controlled acidity of hole-collecting buffer layers on the performance and lifetime of polymer:fullerene solar cells. *J. Phys. Chem. C* **2011**, *115*, 13502−13510.

(21) Lee, S.; Nam, S.; Lee, H.; Kim, H.; Kim, Y. Device performance and lifetime of polymer:fullerene solar cells with UV-ozone-irradiated hole-collecting buffer layers. *ChemSusChem* **2011**, *4*, 1607−1612.

(22) Kim, H.; Shin, M.; Park, J.; Kim, Y. Initial performance changes of polymer/fullerene solar cells by short-time exposure to simulated solar light. *ChemSusChem* **2010**, *3*, 476−480.

(23) Soon, Y. W.; Cho, H.; Low, J.; Bronstein, H.; McCulloch, I.; Durrant, J. R. Correlating triplet yield, singlet oxygen generation and photochemical stability in polymer/fullerene blend films. *Chem. Commun.* **2013**, *49*, 1291−1293.

(24) Wong, H. C.; Li, Z.; Tan, C. H.; Zhong, H.; Huang, Z.; Bronstein, H.; McCulloch, I.; Cabral, J. T.; Durrant, J. R. Morphological stability and performance of polymer-fullerene solar cells under thermal stress: The impact of photoinduced $PC_{60}BM$ oligomerization. *ACS Nano* **2014**, *8*, 1297−1308.

(25) Yang, X.; Loos, J.; Veenstra, S. C.; Verhees, W. J. H.; Wienk, M. M.; Kroon, J. M.; Michels, A. J.; Janssen, R. A. J. Nanoscale morphology of high-performance polymer solar cells. *Nano Lett.* **2005**, *5*, 579−583.

(26) Kim, Y.; Nelson, J.; Zhang, T.; Cook, S.; Durrant, J. R.; Kim, H.; Park, J.; Shin, M.; Nam, S.; Heeney, M.; McCulloch, I.; Ha, C. S.; Bradley, D. D. C. Distorted asymmetric cubic nanostructure of soluble fullerene crystals in efficient polymer:fullerene solar cells. *ACS Nano* **2009**, *3*, 2557−2562.

(27) Manceau, M.; Rivaton, A.; Gardette, J. L.; Guillerez, S.; Lemaitre, N. Light-induced degradation of P3HT-based solar cells active layer. *Sol. Energy Mater. Sol. Cells.* **2011**, *95*, 1315−1325.

(28) Nam, S.; Park, S.; Kim, H.; Lee, J.−H.; Kim, Y. Strong addition effect of charge-bridging polymer in polymer:fullerene solar cells with low fullerene contents. *RSC Adv.* **2014**, *4*, 24914−24921.

(29) Blom, P. W. M.; Mihailetchi, V. D.; Koster, L. J. A.; Markov, D. E. Device physics of polymer:fullerene bulk heterojunction solar cells. *Adv. Mater.* **2007**, *19*, 1551−1566.

(30) Zhou, H.; Yang, L.; You, W. Rational design of high performance conjugated polymers for organic solar cells. *Macromolecules.* **2012**, *45*, 607−632.

(31) Reese, M. O.; White, M. S.; Rumbles, G.; Ginley, D. S.; Shaheen, S. E. Optimal negative electrodes for poly(3-hexylthiophene):[6,6]-phenylC61-butyric acid methyl ester bulk heterojunction photovoltaic devices. *Appl. Phys. Lett.* **2008**, *92*, 053307.

(32) Mihailetchi, V. D.; Blom, P. W. M.; Hummelen, J. C.; Rispens, M. T. Cathode dependence of the open-circuit voltage of polymer:-fullerene bulk heterojunction solar cells. *J. Appl. Phys.* **2003**, *94*, 6849−6854.

(33) Mühlbacher, D.; Scharber, M.; Morana, M.; Zhu, Z.; Waller, D.; Gaudiana, R.; Brabec, C. J. High photovoltaic performance of a low-bandgap polymer. *Adv. Mater.* **2006**, *18*, 2884−2889.

(34) Cook, S.; Ohkita, H.; Kim, Y.; Benson-Smith, J. J.; Bradley, D. D. C.; Durrant, J. R. A photophysical study of PCBM thin films. *Chem. Phys. Lett.* **2007**, *445*, 276−280.
(35) Veldman, D.; Meskers, S. C. J.; Janssen, R. A. J. The energy of charge-transfer states in electron-donor-acceptor blends: Insight into the energy losses in organic solar cells. *Adv. Funct. Mater.* **2009**, *19*, 1939−1948.
(36) Van Hal, P. A.; Janssen, R. A. J.; Lanzani, G.; Cerullo, G.; Zavelani-Rossi, M.; De Silvestri, M. Two-step mechanism for the photoinduced intramolecular electron transfer in oligo(p-phenylenevinylene)-fullerene dyads. *Phys. Rev. B* **2001**, *61*, 075206.
(37) Kim, Y.; Choulis, S. A.; Nelson, J.; Bradley, D. D. C.; Cook, S.; Durrant, J. R. Composition and annealing effects in polythiophene/fullerene solar cells. *J. Mater. Sci.* **2005**, *40*, 1371−1376.
(38) Kim, Y.; Cook, S.; Choulis, S. A.; Nelson, J.; Durrant, J. R.; Bradley, D. D. C. Organic photovoltaic devices based on blends of regioregular poly (3-hexylthiophene) and poly (9, 9-dioctylfluorene-co-benzothiadiazole). *Chem. Mater.* **2004**, *16*, 4812−4818.
(39) Lee, S.; Nam, S.; Kim, H.; Kim, Y. Compression-induced open circuit voltage increase in all-polymer solar cells with lithium fluoride nanolayers. *ACS Sustainable Chem. Eng.* **2013**, *1*, 1280−1285.
(40) Veerender, P.; Saxena, V.; Chauhan, A. K.; Koiry, S. P.; Jha, P.; Gusain, A.; Choudhury, S.; Aswal, D. K.; Gupta, S. K. Probing the annealing induced molecular ordering in bulk heterojunction polymer solar cells using in-situ Raman spectroscopy. *Sol. Energy Mater. Sol. Cells.* **2014**, *120*, 526−535.
(41) Miller, S.; Fanchini, G.; Lin, Y. Y.; Li, C.; Chen, C. W.; Su, W. F.; Chhowalla, M. Investigation of nanoscale morphological changes in organic photovoltaics during solvent vapor annealing. *J. Mater. Chem.* **2008**, *18*, 306−312.
(42) Stavytska-Barba, M.; Salvador, M.; Kulkarni, A.; Ginger, D. S.; Kelley, A. M. Plasmonic enhancement of Raman scattering from the organic solar cell material P3HT/PCBM by triangular silver nanoprisms. *J. Phys. Chem. C* **2011**, *115*, 20788−20794.
(43) Razzell-Hollis, J.; Tsoi, W. C.; Kim, J. S. Directly probing the molecular order of conjugated polymer in OPV blends induced by different film thicknesses, substrates and additives. *J. Mater. Chem. C* **2013**, *1*, 6235−6243.